862 *Biochemistry* **2010,** *49,* 862–871
DOI: 10.1021/bi901723p

BIOCHEMISTRY
including biophysical chemistry & molecular biology
Article

Differential Phospholipid Binding of α-Synuclein Variants Implicated in Parkinson's Disease Revealed by Solution NMR Spectroscopy[†]

Christina R. Bodner,[‡,§] Alexander S. Maltsev,[‡] Christopher M. Dobson,[§] and Ad Bax*[,‡]

[‡]*Laboratory of Chemical Physics, National Institute of Diabetes and Digestive and Kidney Diseases, National Institutes of Health, Bethesda, Maryland 20892-0520 and* [§]*Department of Chemistry, University of Cambridge, Lensfield Road, Cambridge CB2 1EW, U.K.*

Received October 6, 2009; Revised Manuscript Received December 30, 2009

ABSTRACT: Three familial variants of the presynaptic protein α-synuclein (αS), A30P, E46K, and A53T, correlate with rare inherited Parkinson's disease (PD), while wild-type αS is implicated in sporadic PD. The classic manifestation of both familiar and sporadic PD is the formation of fibrillar structures of αS which accumulate as the main component in intraneuronal Lewy bodies. At presynaptic termini, the partitioning of αS between disordered cytosolic and membrane-bound states likely mediates its proposed role in regulation of reserve pools of synaptic vesicles. Previously, we reported on multiple distinct phospholipid binding modes of αS with slow binding kinetics. Here, we report the phospholipid binding properties of the disease variants, viewed by solution NMR in a residue-specific manner. Our results agree qualitatively with previous biophysical studies citing overall decreased lipid affinity for the A30P mutation, comparable affinity for A53T, and an increased level of binding of E46K, relative to wild-type αS. Additionally, our NMR results describe the distribution of lipid-bound states for αS: the population of the SL1 binding mode (residues 3−25 bound as a helix) is augmented by each of the disease variants, relative to wild-type αS. We propose that the SL1 binding mode, which anchors the N-terminus of αS in the lipoprotein complex while the hydrophobic NAC region remains dynamically disordered, is prone to intermolecular interactions which progress toward disease-associated oligomers and fibrils. The elevation of the SL1 binding mode, unchecked by a proportionate population of binding modes incorporating the full N-terminal domain, may well account for the increased toxicity of the A30P, E46K, and A53T disease variants of αS.

In dopaminergic neurons, α-synuclein (αS)[1] partitions between a disordered cytosolic state and helical phospholipid-bound forms. Membrane association of αS likely mediates its role in regulation of reserve pools of synaptic vesicles and dopamine homeostasis, but it is also implicated in the fibril formation propensity (*1*−*7*) and oligomeric pathways (*8*−*10*) of αS, which have been widely studied for their relevance to Parkinson's disease (PD). Three rare autosomal dominant missense mutations of αS, A30P, E46K, and A53T, have been discovered in European kindred with inherited early onset Parkinson's disease (*11*−*13*). Wild-type αS is implicated in the pathology of sporadic PD, which accounts for the vast majority of cases. Whether familial or sporadic, the histological expression of PD is the formation of fibrillar structures of αS which accumulate as the main component in intraneuronal Lewy bodies and neurites (*14*, *15*). The rate of fibril formation in wild-type αS is increased by the presence of dilute lipids and lipid mimetics (*1*, *3*−*6*) but decreased in the presence of high lipid concentrations (*2*−*6*). Among the three disease variants, aggregation kinetics also have been determined in vitro under lipid-free conditions (*16*−*21*) and in catecholaminergic cells with similar results (*22*), but expectations that the mutant proteins would systematically display higher aggregation propensity and faster fibrilization rates were not borne out. Instead, A30P fibrils form more slowly than wild-type fibrils (*16*−*19*), while the E46K and A53T mutations do result in faster fibrillization kinetics (*16*−*22*). Subsequent studies focused on the formation of prefibrillar αS oligomers, which have increasingly been hypothesized as the relevant toxic agent in PD. A number of studies in which preformed oligomers have been added to various membranes have observed vesicle leakage or pore formation, suggesting that neuron damage is the result of membrane disruption by oligomeric αS (*23*−*29*). The rates of conversion among monomeric αS, prefibrillar oligomers, and mature fibrils in the A30P and A53T disease variants are altered from wild-type behavior in a manner that may allow a dangerous accumulation of early oligomeric species (*30*, *31*). The extent of accumulation of E46K prefibrillar species, however, is reduced relative to that of wild-type αS (*32*).

The degree of residual α-helical propensity detected in the N-terminal domain of lipid-free αS, measured by deviations in

[†]This work is funded by the Intramural Research Program of the National Institute of Diabetes and Digestive and Kidney Diseases, National Institutes of Health (Grant DK029047 to A.B.), and by the Leverhulme Trust and the Wellcome Trust (to C.M.D.).

*To whom correspondence should be addressed: 5 Memorial Dr., Bethesda, MD 20892-0520. Phone: (301) 496-2848. Fax: (301) 402-0907. E-mail: bax@nih.gov.

[1]Abbreviations: αS, α-synuclein; BMRB, BioMagResBank; DOPC, 1,2-dioleoyl-*sn*-glycero-3-phosphocholine; DOPE, 1,2-dioleoyl-*sn*-glycero-3-phosphoethanolamine; DOPS, 1,2-dioleoyl-*sn*-glycero-3-phospho-L-serine; EBURP, excitation band-selective, uniform response, pure phase; EPR, electron paramagnetic resonance; HMQC, heteronuclear multiple-quantum coherence; HSQC, heteronuclear single-quantum coherence; LUV, large unilamellar vesicle; NAC, nonamyloid component; NOE, nuclear Overhauser effect; NMR, nuclear magnetic resonance; PD, Parkinson's disease; REBURP, refocused band-selective, uniform response, pure phase; SUV, small unilamellar vesicle; TROSY, transverse relaxation-optimized spectroscopy; WT, wild type.

 Published on Web 12/30/2009 © 2009 American Chemical Society

chemical shifts from random coil values, has been used as an indicator to study structural differences between the disease variants (*33*, *34*). Partitioning of each of the constructs to a helical, bound form in the presence of lipid mimetics has also been characterized (*35*−*37*). Here again, the simple model that supposes that structure adopted in a membrane-bound conformation of αS would be protective against aggregation is not supported by the mutant αS data. The A30P variant does display lower helical propensity and disrupted membrane interactions; however, E46K partitions more easily to the bound state, while the A53T mutation exhibits a lower helix propensity combined with a membrane affinity comparable to that of the wild type (*17*, *19*, *38*). Clearly, a more detailed picture is needed to reconcile the fact that none of these hypothesized indicators (fibril formation rates, oligomer accumulation, residual helical conformation, or membrane affinity) satisfactorily accounts for the potency of the αS disease mutants.

For wild-type (WT) αS, we recently described distinct phospholipid binding modes that exhibit slow exchange kinetics (*39*). Interestingly, evidence of slow exchange kinetics is also found in the study of interactions between fatty acids and WT αS (*9*). Though the bound modes are observed only indirectly because the large size and/or dynamic behavior of the lipid-bound states makes them inaccessible to solution NMR experiments, the bound segments of the protein can be resolved to the level of individual residues. Here we investigate the membrane interactions of the disease variants of αS in an analogous manner. The results reveal for each of the variants a redistribution of bound modes from that observed for WT αS. The implications lead us to propose a new mechanism by which αS is protected from or predisposed to the early events of aggregation.

EXPERIMENTAL PROCEDURES

Protein Expression and Purification. Human wild-type αS with ^{15}N and ^{2}H isotopic enrichment was expressed and purified by anion-exchange chromatography as previously described (*39*). A30P, E46K, and A53T αS were expressed from recombinant plasmids produced by mutagenesis of the wild-type sequence using Quikchange mutagenesis reagents and standard PCR techniques. All complementary primers were synthesized by the U.S. Federal Drug Administration (FDA). DNA sequencing verified the presence of the desired mutations (FDA, Bethesda, MD). The disease variants were purified in the same manner as the WT protein. Purified protein was dialyzed into water and lyophilized for storage.

Preparation of Lipid Vesicles. Phospholipids were purchased as a lyophilized mixture (5:3:2 DOPE/DOPS/DOPC) from Avanti Polar Lipids (Alabaster, AL) and used without further purification. A 15% (w/v) stock solution of small unilamellar vesicles (SUVs) was prepared as previously described (*39*). More dilute solutions of SUVs were made from the stock solution as necessary for experimental purposes. Large unilamellar vesicles (LUVs) were prepared by multiple cycles of extrusion using the Avanti Polar Lipids mini-extruder through membranes with a 100 nm pore size, resulting in relatively uniformly sized vesicles with an average diameter of 140 nm, as judged by dynamic light scattering on a Malvern Zetasizer (model ZEN3601) instrument. ^{1}H NMR resonances of the terminal alkane moieties of the fatty acid chains in LUVs exhibit more rapid transverse relaxation and correspondingly larger line widths than the corresponding resonances in SUVs (Figure 4 of the Supporting Information).

NMR Spectroscopy. NMR spectra were recorded at 293 K on a Bruker spectrometer operating at a ^{1}H frequency of 600 MHz equipped with a cryogenic probe. Data were processed and analyzed using NMRPipe (*40*). Samples were prepared from lyophilized protein dissolved in 20 mM Na_2HPO_4 (pH 6.0), a 94% H_2O/6% D_2O mixture, and 0.02% NaN_3. Concentrations were determined by UV−visible spectra using an extinction coefficient for αS (ε_{280}) of 5120 M^{-1} cm^{-1} and were confirmed via one-dimensional (1D) proton NMR by comparison of signal intensity to a reference at a known concentration.

No prior backbone amide $^{1}H-^{15}N$ assignments for disordered αS at nearly neutral pH were available in the BioMagResBank (BMRB), and our assignments appear to differ somewhat from those shown in several previously published, annotated spectra. In particular for residues lying within the KTKEGV repeat motifs of αS, chemical shift degeneracy can result in ambiguity in assignment by conventional techniques. Therefore, extensive sequential NOE correlations observed for αS in the presence of lipids (*39*) were used to confirm the sequence assignments of WT αS in our work. On the other hand, our ^{15}N chemical shift values are in excellent agreement with those reported by Bermel et al. on the basis of direct ^{13}C detection experiments (*41*). Resonance assignments for A30P, E46K, and A53T αS were made by the transfer of the very similar wild-type assignments. Small chemical shift changes were observed only for those residues in the immediate vicinity of the mutation site, and assignments of these residues were again verified by sequential cross-peaks in three-dimensional (3D) HMQC-NOE-HMQC spectra, described below. Complete $^{1}H-^{15}N$ assignments (residues 3−140, excluding proline residues) for disordered WT, A30P, E46K, and A53T αS have been deposited in the BMRB (accession numbers 16543, 16546, 16547, and 16548, respectively) and are available as Supporting Information.

For experiments in which lipids were titrated into the sample, HSQC spectra were recorded with a data matrix consisting of 1280 (t_2, ^{1}H) × 448 (t_1, ^{15}N) complex points ($t_{2,max}$ = 152 ms, and $t_{1,max}$ = 334 ms). The ^{15}N TROSY experiments for measurement of R_2^T (*42*, *43*) were conducted as interleaved experiments with 12 T_2 delays (20, 30, 50, 70, 90, 120, 150, 180, 220, 270, 400, and 500 ms) and acquisition times matching those of the regular HSQC experiments. 3D HMQC-NOE-HMQC spectra were recorded with a mixing time of 100 ms, as data matrices consisting of 2048 (t_3, ^{1}H) × 84 (t_2, ^{15}N) × 84 (t_1, ^{15}N) complex points ($t_{3,max}$ = 106 ms, $t_{2,max}$ = 60.8 ms, and $t_{1,max}$ = 60.8 ms). Amide-selective EBURP and REBURP pulses (*44*), of 1.8 ms duration each and centered at 8.3 ppm, were used for both experiments.

RESULTS

Relative Phospholipid Binding Affinities of αS Variants. The equilibrium partitioning of αS between phospholipid-bound and free populations has been investigated for the wild-type protein and each of the disease variants upon addition of small unilamellar vesicles (SUVs). All vesicles used in our study consist of a 5:3:2 DOPE:DOPS:DOPC molar ratio, maintaining a net negative charge and lipid moieties native to the synaptic environment (*45*). The size and curvature of our model SUVs approximate those of synaptic vesicles. These vesicles are added to a solution of αS, and their impact upon the two-dimensional NMR

spectrum is monitored in a residue-specific manner (Figure 1A, shown for a small section of the two-dimensional $^{1}H-^{15}N$ correlation spectrum of E46K αS). The fractional attenuation of signal intensity for any given backbone amide $^{1}H-^{15}N$ cross-peak in the heteronuclear single-quantum correlation (HSQC) spectrum indicates that a corresponding fraction of the αS population is engaged in phospholipid binding in a mode in which the amide group of this residue exhibits line widths too broad to be observed in the HSQC spectrum (*39*). The retained signal intensity arises both from αS molecules that are fully lipid-free and from αS residues that are themselves free and dynamically disordered, even while an "upstream" (more N-terminal) segment of the same protein molecule is lipid-bound with its NMR signals unobservable. In both cases, the observed chemical shifts are identical to those observed for αS in the absence of lipids because they arise from αS residues in the dynamically highly disordered state.

When the signal attenuation in the $^{1}H-^{15}N$ HSQC spectrum is viewed as a function of residue number (Figure 1B), the spectrum is dramatically impacted by the presence of lipids, both for WT αS and for the three disease mutants, even at very low lipid:protein molar ratios (near unity). This result is reminiscent of the signal attenuation previously noted for aS in the presence of equimolar quantities of various fatty acids (*9*). As observed for WT αS (*39*), each of the disease variants shows a differential degree of binding across its sequence, with the N-terminal residues (segments containing ca. the first 10, or the first 24, amino acids are distinguished in particular) partitioning most strongly into the NMR-invisible lipid-bound state. We term this first bound state, comprised of a short bound α-helix followed by dynamic disorder in residues ~25−140, SL1. A second bound state, which we term SL2, engages the full N-terminal domain, up to residue ~100, in the α-helical conformation, while the 40 residues of the C-terminal tail remain flexible in solution. Akin to the wild-type scenario, each of the αS variants binds to SUVs with exchange kinetics that are slow on the NMR time scale, evidenced by the lack of significant broadening or shifting of any of the HSQC resonances, even while the intensities are attenuated due to lipid binding. The kinetics are investigated in detail below, but we point out here that the modes of binding are very similar to those previously described for WT αS (*39*).

To ensure that the binding modes observed for the αS variants are not the result of altered vesicle morphology induced by the mutant proteins, two additional experiments were conducted. In the first, we tested whether large unilamellar vesicles (LUVs) of the same composition as our SUVs alter the lipid binding profile of αS (Figure 2 of the Supporting Information). For the first 100 residues, the attenuation pattern is essentially the same between the two vesicle sizes, indicating that the binding modes are insensitive to the initial vesicle diameter. In a second set of experiments, the attenuation of the signal for mixed samples of WT and A30P αS was monitored (Figure 3 of the Supporting Information). Equimolar amounts of isotopically labeled WT and unlabeled A30P αS, or the reverse labeling scheme, were added to the lipid vesicles. As expected, WT and A30P αS compete (with A30P having a lower affinity) for lipid binding sites, affecting the degree of attenuation observed for each protein. However, the patterns of attenuation for WT and A30P αS remain unchanged in the presence of the other protein. While the lipid morphology may be disrupted by the presence of αS [as observed by cryo-electron microscopy on samples of αS added to the same SUVs (*39*)], results obtained for the mixed

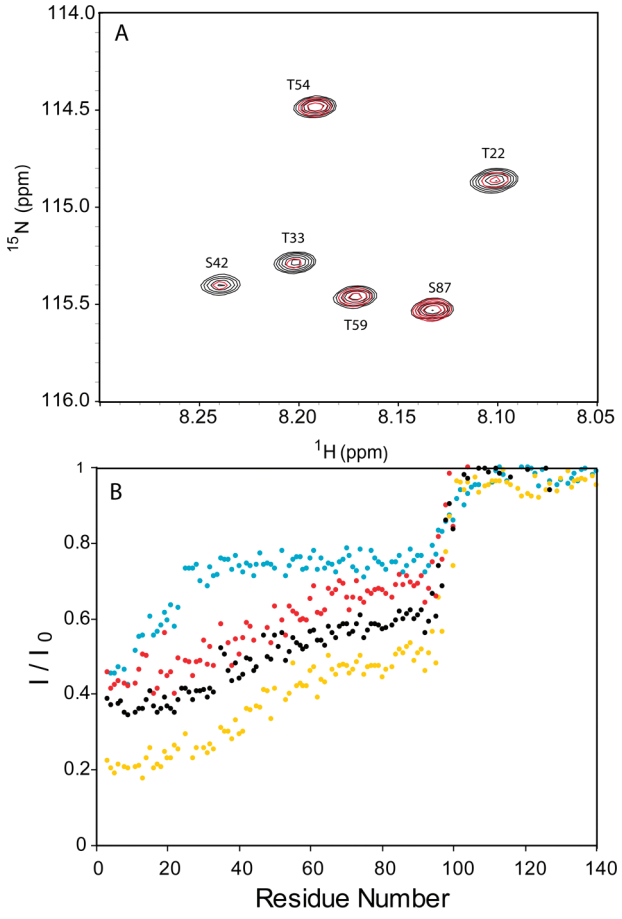

FIGURE 1: Signal attenuation observed in the $^{1}H-^{15}N$ HSQC spectrum of αS corresponds to the fractional population of αS engaged in phospholipid binding at a particular residue location. (A) Cross section of the $^{1}H-^{15}N$ HSQC spectrum of E46K αS, in the absence (black) and presence (red) of 0.03% SUVs. (B) Fractional signal attenuation of wild-type (black), A30P (blue), E46K (gold), and A53T (red) αS in the presence of 0.03% (w/v) SUVs plotted as function of residue number. The protein concentration for all series is 300 μM, such that the lipid to protein molar ratio is approximately 4:3.

samples indicate that alterations in lipid morphology are not responsible for the different modes of binding observed for each of the αS variants.

The lipid binding affinity of the first 10 N-terminal residues of A30P αS approaches that of the wild-type protein. A segment containing residues 11−23 exhibits progressively increasing resonance intensity, corresponding to an increasing fraction of the disordered population, and the attenuation shows a flat profile at ~75% intensity relative to the lipid-free state beginning from around residue 25, a point just preceding the mutation site. This indicates that for a fraction (~25%) of A30P αS residues 25−100 are in a lipid-bound state, whereas for the remaining 75% of the protein, this part of the chain is fully disordered, in a random coil-like state. The weaker binding compared to that of WT for the majority of the N-terminal residues is expected on the basis of the decreased helix propensity of the A30P variant, as WT binds lipids in an α-helical mode. Proline is known to disfavor α-helix formation both because it has no amide proton that can engage in hydrogen bonding and because its cyclic side chain locks the φ backbone torsion angle at approximately −75°. While the overall bound population of A30P αS is only modestly reduced (54% bound) relative to the wild-type population (63% bound), the redistribution of bound modes is more striking:

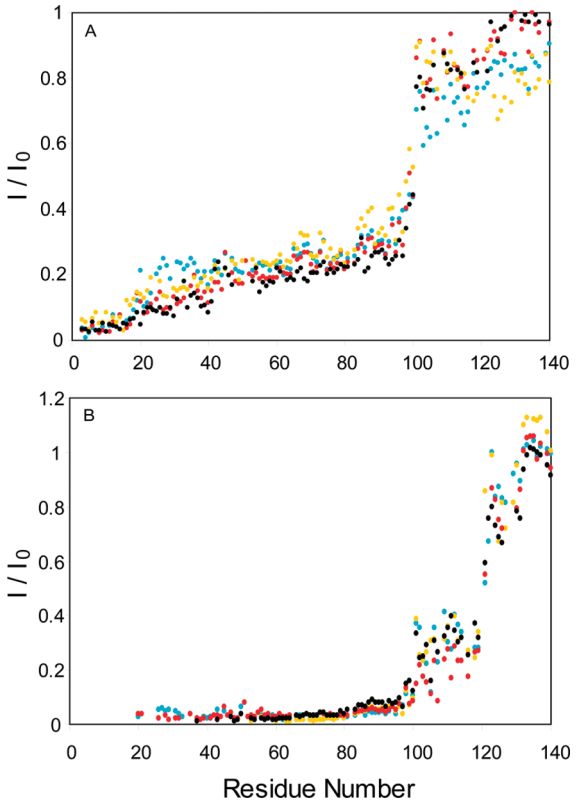

FIGURE 2: Effect of increased lipid concentrations on the binding of αS and its disease variants. Fractional intensity in the HSQC is shown for WT (black), A30P (blue), E46K (gold), and A53T (red) αS in the presence of 0.25 (A) or 2.0% SUVs (B). The lipid:protein ratio is 11:1 or 86:1, respectively. N-Terminal residues whose intensities are too weak for reliable detection have been omitted. For C-terminal residues, which show slightly heterogeneous chemical shifts in the 2.0% SUV condition (see the text), fractional intensities plotted in panel B reflect the attenuation of the nonshifted resonance.

inspection of the curves for WT and A30P αS (Figure 1B) reveals that the ratio of SL1 to SL2 binding modes is greatly increased by the mutation.

In reality, the designation of SL1 and SL2 is a simplified classification comprising a number of different modes evident in the intensity profiles, each the result of a discrete set of contiguous, bound residues (always beginning at the N-terminus). Inspection of the A30P and E46K data series in particular shows a number of clear "steps" in the attenuation profile (Figure 1B). Even though such steps are not as pronounced for the WT and A53T series at low lipid concentrations, they are readily seen at higher lipid levels (Figure 2). These intermediate-bound modes, terminating between residues 25 and 100, constitute distinct modes of αS that are differentially populated by WT αS and each of the disease mutants. Considering that none of the resonances shows line broadening or resonance shifting relative to lipid-free αS, each of these modes is separated by an energy barrier sufficiently large to give rise to the slow kinetics observed. In practice, accurate measurement of these modes is limited by the signal-to-noise ratio of the experiment and some instances of signal overlap in the HSQC spectrum, which becomes progressively more problematic for strongly attenuated resonances in the vicinity of much less attenuated signals from residues closer to the carboxy terminus. For this reason, the following analysis is focused on the simplified depiction of SL1, SL2, and their relative population ratios. The total population of bound αS (under any mode) corresponds to the fractional attenuation of the most

Table 1: Disease Variant Equilibrium Populations under Dilute Lipid Conditions[a]

	total bound population[a]	SL1 fractional population[b]	SL2 fractional population[c]	ratio (SL1:SL2)
WT αS	0.63	0.21	0.43	0.49
A30P αS	0.54	0.30	0.25	1.2
E46K αS	0.81	0.26	0.53	0.49
A53T αS	0.58	0.24	0.33	0.73

[a]Derived from attenuation data of Figure 1B. [b]Difference between fractional attenuation of residues 3−9 and average fractional attenuation of residues 65−80. [c]Average fractional attenuation for residues 65−80.

N-terminal segment and is compared for WT αS and each of the disease variants in Table 1. The fraction of αS bound as SL2 has been determined as the average fractional attenuation for residues 65−80, where the attenuation profiles in Figure 1B show remarkable consistency. The fraction of αS bound as SL1 was calculated by subtracting the SL2 fraction from the average fractional attenuation observed for residues 3−9 (i.e., yielding the population that is bound at the N-terminus but not bound at positions 65−80).

The E46K αS variant displays an overall higher level of lipid partitioning of SL1, SL2, and all intermediate modes, relative to that of the wild type. This result is readily understood from the viewpoint of electrostatics, since a negative glutamate is replaced with a positive lysine, favoring interactions with the SUV lipid mixture which carries a net negative charge. The mutation raises the net charge of the 100-residue N-terminal domain from +4 to +6. Though quantification of the simplified SL1:SL2 ratio in the E46K mutant appears to be essentially the same as for WT, the increased affinity nevertheless increases the population of SL1 by ~25%.

Among the three disease variants, the A53T mutation has the most subtle effect upon lipid binding. The attenuation profile (Figure 1B) is only slightly offset from the WT curve, correlating to a modest elevation of the SL1 binding mode, even while the overall binding affinity (absolute fraction bound under any mode) appears similar to that of the wild type. To a lesser degree than for the A30P mutation, A53T also exhibits an increase in the ratio of SL1- to SL2-bound populations.

The results above describe the lipid-limited case, where the different bound modes are in competition for phospholipid targets. The bound populations of αS have also been quantified at an intermediate lipid concentration (lipid:αS ratio of ~11) and under excess lipid conditions (lipid:αS ratio of ~86). As before, the attenuation of the signal in the HSQC spectrum is used as a reporter of binding in a site-specific manner (Figure 2). Particularly at the highest lipid concentrations, these measurements are made more difficult because the signal-to-noise ratio suffers for the highly attenuated resonances. Additionally, the intensity ratios determined for resonances of the C-terminal tail become less consistent as these peaks show small heterogeneities in their shifts under these high-lipid conditions, manifesting themselves as multiple small distinct shoulders or very proximate weaker resonances (data not shown). These chemical shift heterogeneities result in some scatter of the intensities measured for this region. Nevertheless, these attenuation patterns show the excess lipid condition to be a continuous extension of the lipid-limited case and allow us to compare trends between the αS variants.

At a weight by volume lipid concentration of 2.0% (lipid:protein molar ratio of 86), reliable intensities for the ~20

N-terminal residues can no longer be detected for any of the variants. Stronger lipid partitioning of E46K αS persists even with the lipid limiting condition removed, as residues up to position 53 are unobserved for this variant (Figure 2B). For A30P αS, deficient binding of residues 24−36 persists at the intermediate lipid concentration (Figure 2A) and at the highest lipid concentration, curiously, shows a higher free fraction for this segment than residues located adjacently in the C-terminal direction. This suggests that the helix-perturbing mutation also can result in a high level of local dynamic disorder for these residues, even while the remainder of the N-terminal domain remains tightly bound. The fact that these resonances are observed and exhibit random coil-type line widths is further evidence of the "jointed" lipid binding of αS, which displays sharp boundaries between ordered and highly flexible residues. In spite of these observations, other binding features that differentiate the αS variants at low lipid concentrations are largely absent at the higher lipid concentrations investigated. In particular, no appreciable free population persists for any of the variants in excess lipids. If the factors that dispose αS toward disease are linked to its capacity to bind lipids, it is likely that deficits would be most acute under competitive binding conditions, as observed in Figure 1.

Kinetics of Binding Are Affected by αS Mutations. The altered steady state bound populations of αS disease variants could be due to changes in the lipid association rate, dissociation rate, or both. As shown previously for WT αS (*39*), the lipid association rate can be conveniently probed as a contribution to the decay of signal in a TROSY-HSQC experiment when monitoring the ^{15}N transverse magnetization decay rate R_2^T. Such a measurement is only possible when the free−bound forward transition occurs on a time scale not much slower than the inverse of the intrinsic transverse relaxation rate of the random coil state and is a remarkable feature of the long-lived exchangeable states of αS and the slow transverse relaxation of dynamically disordered αS. An analogous set of transverse relaxation data was acquired for each of the disease variants.

In the slow-exchange limit, the observed R_2^T equals the sum of the R_2^T value of the highly mobile lipid-free random coil state, $R_2^T{}_{random\_coil}$, and the forward rate of the free−bound transition, k_{on}. R_2^T values in the lipid-free state for αS are very low, ~3 s^{-1} (Figure 3), allowing straightforward detection of even relatively small contributions resulting from k_{on}. With the exception of several residues for which the intrinsic random coil hydrogen-exchange rate is highest (*46*) and for which this type of exchange impacts the apparent R_2^T value, transverse relaxation rates in the absence of lipid are quite uniform and very low, in agreement with a highly mobile, disordered random coil-like conformation (*33*, *47*−*49*). In the presence of lipids, a significant increase in the transverse decay rate is observed for residues 1−100 (Figure 3), indicative of k_{on} values in the range of 3−6 s^{-1}.

The rates measured for the 40 residues of the C-terminal tail are highly uniform, corresponding to T_2 values of ~350 ms, regardless of the presence of lipids or any of the three point mutations. As expected, the presence of dilute lipids (lipid:αS molar ratio of ~1.3) elevates the effective R_2^T measured for the N-terminal domain for WT and all variants of αS. Comparison of the rates measured for WT, E46K, and A53T αS reveals minimal differences between the data series, signifying nearly identical association rates for these variants (plots not shown, but rates summarized in Table 2). In the case of E46K αS, for which the equilibrium constant is increased (i.e., the bound fraction is increased), this unaltered association rate specifies that the lipid dissociation rate must be slower than that of the wild type. In contrast, the A30P mutation results in lower R_2^T values relative to that of WT αS under identical lipid conditions (Figure 3). Taking the difference between the effective R_2^T and the intrinsic transverse relaxation rate measured for αS in the absence of lipids, we obtain the lipid association rate, k_{on}, for both WT and A30P αS in a site-specific manner. Across the N-terminal region, a 2−3-fold reduction in the k_{on} rate is observed for A30P relative to WT αS. With the equilibrium-bound fraction also known (Figure 1B), the dissociation rate is derived.

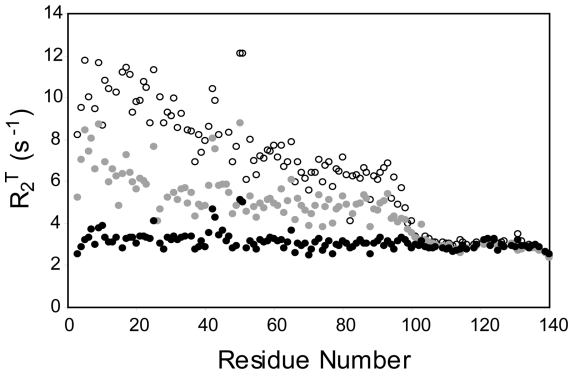

FIGURE 3: Transverse relaxation rates of the ^{15}N TROSY component, R_2^T, measured for 600 μM WT αS (white circles) or A30P αS (gray circles) in the presence of 0.06% SUVs. The rates measured for WT αS in the absence of lipids are also plotted (black circles).

Table 2: Lipid Association and Dissociation Rates for αS Variants[a]

	bound fraction	experimental k_{on} (s^{-1})	calculated k_{off} (s^{-1})
WT αS	0.60 ± 0.01	6.1 ± 0.6	4.1 ± 0.4
A30P αS	0.28 ± 0.02	1.9 ± 0.5	4.8 ± 1.4
E46K αS	0.75 ± 0.01	5.7 ± 0.6	1.9 ± 0.2
A53T αS	0.51 ± 0.03	5.7 ± 0.8	5.5 ± 0.8

[a]Reported as the average values for residues 26−33 under the low-lipid conditions described in the legend of Figure 3.

The average rates and equilibrium populations of each of the αS variants are reported for a stretch of residues near the N-terminus, V26−T33, inclusive. Located in the beginning of the "SL2" region, this set of representative residues is approximately flat in their attenuation profiles and also exhibits relatively consistent R_2^T values. In the A30P construct, the association rate for this region is decreased, as mentioned above, but the calculated dissociation rate is insensitive to the mutation. The lowered binding affinity then must be attributed entirely to a slower k_{on}. An opposite effect on kinetics is observed for the E46K variant. Here, the mutation affects the dissociation rate, k_{off} (slowing it by a factor of >2), while k_{on} is only modestly modified from the wild-type rate. Further discussion of the possible sources of altered kinetics is presented later.

NOE Transfer in the "Dark State". Previously, H^N−H^N NOE correlations of the dark state of αS were measured via 3D NOESY experiments (*39*). Analogously, 3D HMQC-NOE-HMQC spectra were acquired for each of the disease variants in the presence of 0.06% lipid (lipid:protein molar ratio of ~1.3). Because NOE experiments store magnetization along the longitudinal axis, protein molecules that associate as a bound complex and dissociate within the NOE mixing time of the experiment retain the "memory" of their bound state and display

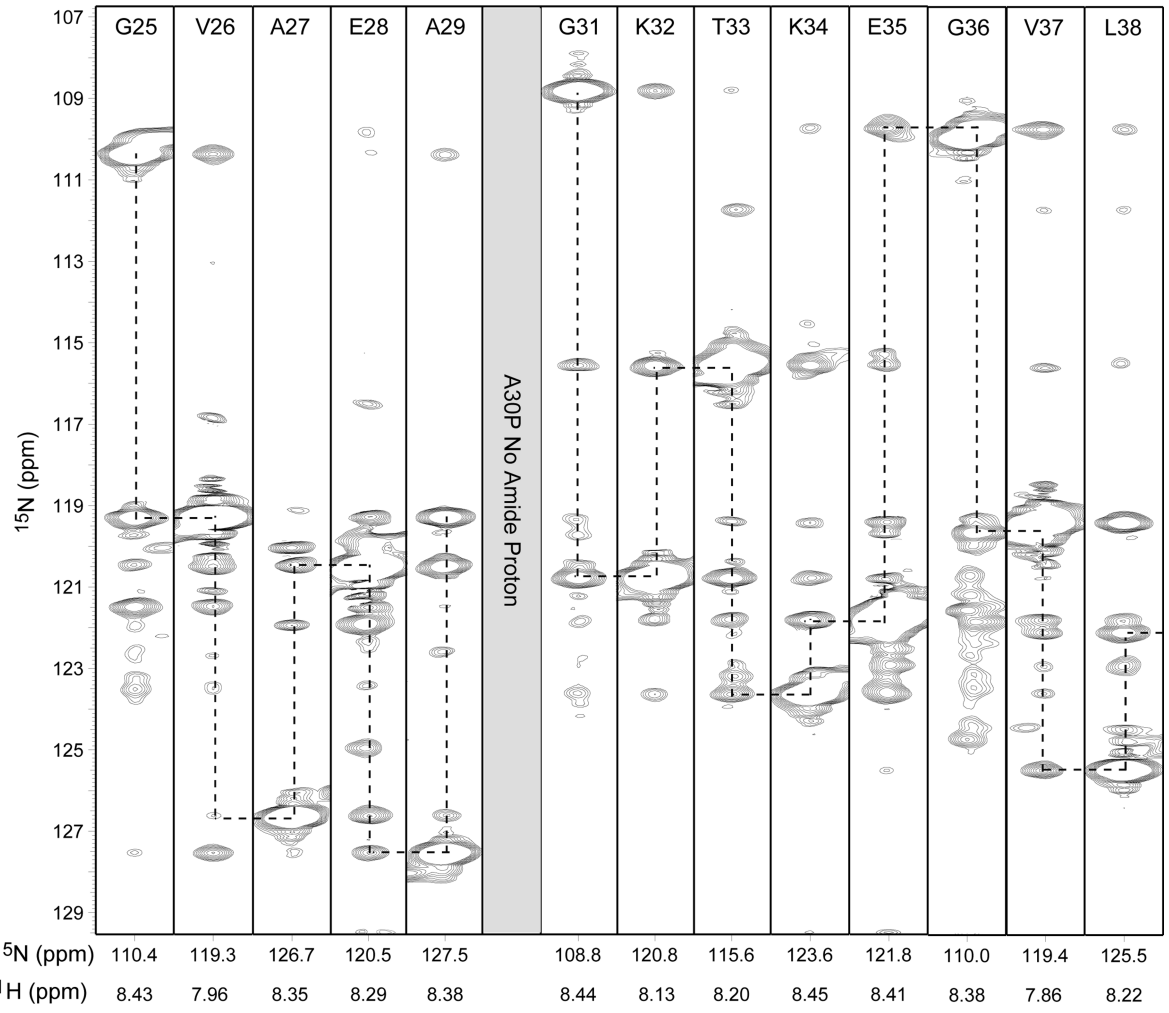

FIGURE 4: Series of strip plots showing $^1H-^1H$ amide NOEs for residues 25−38 (excepting P30) of 600 μM A30P αS in the presence of 0.06% SUVs. Strips are taken orthogonal to the ^1H frequency axis of a 600 MHz 3D HMQC-NOESY-HMQC spectrum. The NOE mixing time was 100 ms.

cross-peaks that report on NOE magnetization transfer that took place during that time. As found for the 40 C-terminal residues, and previously observed for WT αS in the absence of lipids (*39*), NOE magnetization transfer for the disordered, random coil state of αS is very slow, contributing minimally to cross-peaks between the amide protons. NOE cross-peaks observed for the 100 N-terminal residues in the presence of lipids therefore are dominated by the structure and dynamics in the lipid-bound state.

In comparison to lipid-bound WT αS, which displays numerous i to $i \pm n$ connectivities (up to $n = 6$) due to extensive spin diffusion in the dark state (*39*), the NOE cross-peak pattern in A30P αS is sharply reduced. Throughout the SL2 region, cross-peak intensity ratios, relative to the diagonal peak of a given residue, are approximately 2-fold weaker than the corresponding cross-peaks of WT αS under the same conditions (data not shown). This result agrees well with the attenuation data of Figure 1B which shows nearly twice the SL2 population for WT versus A30P αS and simply reflects the lower signal-to-noise ratio for cross-peaks arising from a reduced bound population in the mutant. However, in the N-terminal segment preceding position 30, the pattern of cross-peaks observed is additionally affected by the mutation. Figure 4 shows a number of strips taken from the 3D HMQC-NOE-HMQC spectrum for residues G25−L38 of the A30P variant. In contrast to what was previously seen for WT αS, in the vicinity of the mutation site, the monotonic decrease in cross-peak intensities for increasing n is not observed in all cases. Instead, $i-i \pm 3$ cross-peaks show higher intensities than $i-i \pm 1$ and $i-i \pm 2$ cross-peaks in some instances [for example, see the mirrored cross-peaks between V26 and A29 that are approximately 6 times more intense than those between V26 and A27 (Figure 4)]. Although quantitative interpretation of cross-peak intensities in terms of interproton distances is complicated by the unknown degree of spin diffusion, this finding strongly suggests a V26 H^N-A29 H^N distance that is comparable to the distance of 2.8 Å between sequential amide protons in an α-helix, and a considerably longer sequential V26 H^N-A27 H^N distance. Short distances between amide protons of residues i and $i + 3$ are characteristic of turn-type conformations but without additional structural information are insufficient for the determination of the specific turn type.

E46K αS also shows significant variation from WT in its H^N-H^N NOE cross-peak pattern. The overall number of cross peaks detected is again reduced for the E46K mutant (Figure 5) relative to WT αS. However, in contrast to the A30P mutant, attenuation of intensities is comparable to what is seen in WT αS and therefore cannot be attributed to a lower population of dark state αS. Instead, the lower NOE cross-peak intensity is caused by its slower k_{off} rate relative to that of WT αS (Table 2), which causes fewer molecules to undergo a transition from free to

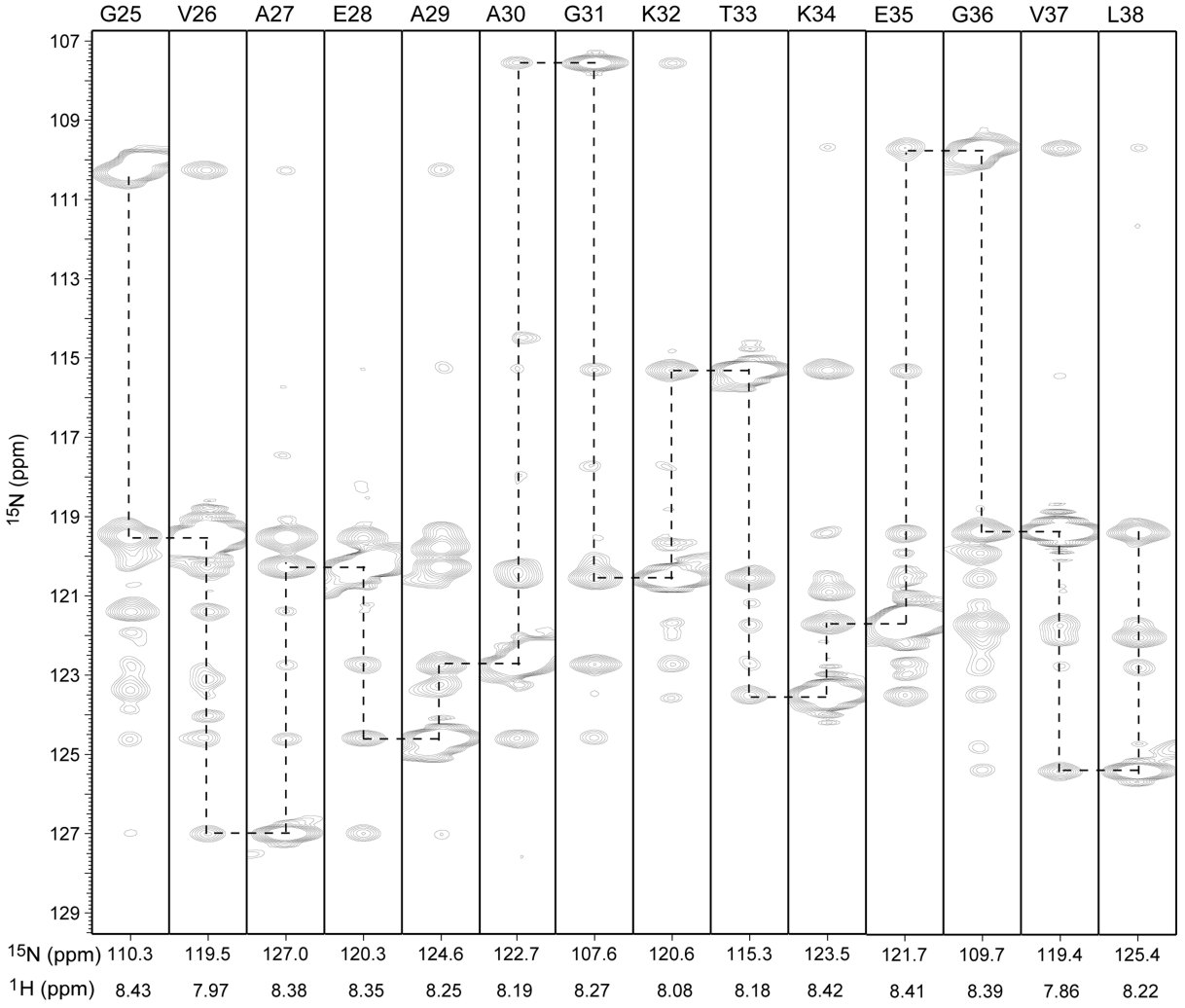

FIGURE 5: Series of strip plots showing $^{1}H-^{1}H$ amide NOEs for residues 25−38 of 600 μM E46K αS in the presence of 0.06% SUVs. Strips are taken orthogonal to the ^{1}H frequency axis of a 600 MHz 3D HMQC-NOESY-HMQC spectrum. The NOE mixing time was 100 ms.

bound to free in the 100 ms NOE mixing time of the experiment. This effect is partially offset by the increased level of binding of the E46K variant, but nevertheless, cross-peaks are somewhat weaker for this mutant relative to WT and also relative to the A53T variant (Figure 1 of the Supporting Information). Intriguingly, monotonic decay of cross-peaks with an increasing n appears to be suspended for the region from G25 to A29 in the spectrum of E46K αS: the $i + 4$ cross-peak in the G25 strip appears twice as intense as the $i + 3$ cross-peak. As in the A30P mutant, this suggests that this region may engage in motifs other than the canonical helix observed for the rest of the N-terminal domain. However, the clear signature of extensive spin diffusion along the protein backbone prevents more quantitative interpretation of the NOE data.

$H^{N}-H^{N}$ NOE transfer in A53T αS is observed with an intensity pattern very similar to that of WT, without evidence of helical breaks either in the region of residues 25−30 or in the vicinity of the mutation site (Figure 1 of the Supporting Information).

DISCUSSION

In addition to their value in yielding potential insights into the molecular mechanisms of Parkinson's disease pathology, comparison studies of the αS disease variants also highlight important biophysical aspects of the native lipid interactions of αS. The intensity and relaxation data reported here reveal how the mutation sites of αS affect its behavior both locally and globally. Studies that have employed circular dichroism, isothermal titration calorimetry, or other methods that lack site-specific resolution have been limited to making more general conclusions about the global affinity of αS and its variants for lipid vesicles. Fluorescence and EPR studies have been able to report on a number of specifically labeled sites within αS (*50*−*56*), but single- or double-site labeling is both cumbersome and potentially perturbing to the native binding. The finer lens of solution NMR is ideal for examining the differential effects of the disease-associated mutations on αS−lipid binding. A prior NMR study of binding of αS and two of its mutants, A30P and A53T, to lipid vesicles of various compositions observed spectral intensities in terms of average lipid binding capacity of the protein's ~100 N-terminal residues, and its 40-residue acidic C-terminal tail (*35*, *57*). When using this coarse distinction, the results presented here fully agree with the earlier conclusions that on average the lipid binding propensity of the 100 N-terminal residues is higher than for the C-terminal tail, with little impact from the disease mutations. However, when analyzing the data in the site-specific manner employed in this study, we see considerable differences. For example, we find that the 12 N-terminal residues of the A30P mutant retain high lipid binding affinity and that the N-terminal domain region following the mutation site

(residues G31−L100) binds in an "all-or-nothing" fashion, yielding a very flat attenuation pattern for this region, whereas for WT and the other disease variants, the level of attenuation decreases when moving in the C-terminal direction. The latter points to distinctly different stable binding modes, which terminate at different locations in the G31−L100 segment. For the 40 C-terminal residues, no lipid binding is observed at low lipid:αS ratios, but as previously observed for WT, considerable resonance attenuation is seen at high ratios, with distinct steps at locations that coincide with the positions of proline residues (at P120 and P128). No large differences between the lipid binding characteristics of WT and the three mutants are seen at high lipid:protein ratios, however.

Forces Driving the Binding Kinetics of the αS−Lipid Particle. The opposite effects on the kinetics of lipid binding induced by the A30P and E46K mutations shed light on the forces driving the αS−lipid interaction. The lipid association rate is sensitive to the helical propensity of αS (which is impaired by the A30P mutation), while the dissociation rate is more sensitive to electrostatic interactions (which are promoted by the E46K mutation). Binding can be viewed as a two-step process of encounter and reaction. In the case of binding of αS to lipid, the overall observed rate appears to be governed by the reaction after encounter with lipids, since the A30P mutation can slow the association rate. This inhibition of k_{on} is likely caused by the inability of free A30P αS to transiently adopt an ideal α-helical conformation encompassing the mutation site. Formation of the α-helical secondary structure alone, however, is insufficient to provide the driving force for the association of the αS−lipid particle since there is little free energy difference between backbone residues forming intramolecular hydrogen bonds to stabilize the αS helix and the same backbone residues forming hydrogen bonds to solvent molecules, resulting in the modest α-helical propensity observed for αS in free solution (*33*). Consequently, the interaction of hydrophobic side chains of the N-terminal domain of αS with the hydrocarbon tails of the lipids is the likely driving force of association. Lowering the population of a helical "transition state" which exposes its hydrophobic side chains in a pattern ready for lipid association will therefore slow the lipid binding rate. Once αS is bound to the negatively charged lipids, however, electrostatic interactions dominate the stability of the particle. The favorable changes in electrostatics in the E46K variant when bound to negatively charged lipids slow the dissociation of αS from the particle. Since charge−charge attraction or repulsion is effective only over relatively short distances (the Debye length is approximately 12 Å for aqueous samples at low salt concentrations), the dissociation rate is more likely to be impacted by electrostatics than the encounter rate between the helical state of αS and lipids.

The low lipid:protein stoichiometry (approximately 2:1) of the bound complex necessarily results in a highly charged bound complex. The 100 N-terminal residues of αS carry a net charge of +4, while 30% of the lipids in the DOPE/DOPS/DOPC SUVs are negatively charged. Although the lipid composition of the αS−lipid particles is not precisely known, even if the αS-binding lipids were restricted to the negatively charged DOPS component, the core of the resulting particle carries a substantial positive charge. For higher-order oligomers, the particle likely cannot be sustained without substantial charge compensation. Attenuation of the C-terminal residues at higher lipid concentrations (see, e.g., Figure 2) indicates an interaction of this tail for a fraction of the proteins in the particle and may reflect the association of the negatively charged tail (net charge of −13) with the bound complex as a means of neutralizing the positive core. Indeed, the C-terminal residues of the E46K variant show more attenuation than those of WT or other αS variants under dilute lipid conditions (Figure 1B). A recent study also notes an increased number of C-terminal to N-terminal contacts in the absence of lipids for the E46K mutant, as determined by solution NMR paramagnetic relaxation enhancement measurements (*34*).

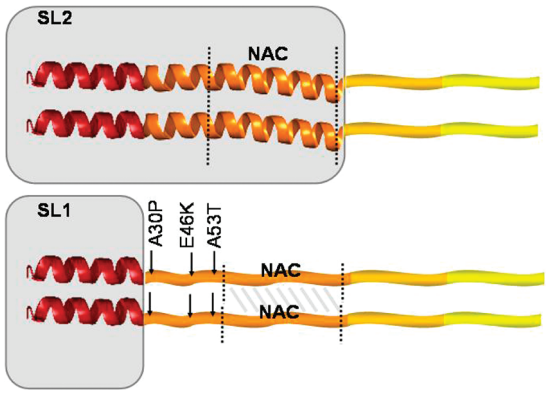

FIGURE 6: Schematic depicting the proposed increased vulnerability of αS to self-association when engaged in the SL1 binding mode vs SL2. The A30P and A53T disease mutations both increase the relative population of SL1, for which a long unstructured stretch of N-terminal residues (including the hydrophobic NAC region) is exposed.

Possible Mechanism for the Potency of A30P, E46K, and A53T Mutations. Under lipid-limited conditions, partitioning of the distinct phospholipid binding modes of αS is affected by each of the three known disease mutations. The higher, comparable, and lower total lipid affinities of E46K, A53T, and A30P αS variants have, to this point, been difficult to understand with respect to PD etiology. This paradox, however, appears to be largely resolved when considering the relative ratios of the different lipid-bound states of αS, in addition to global binding. For each of the disease variants, a redistribution of bound modes, relative to wild-type αS, is observed.

The absolute fraction of αS bound as SL1 is significantly increased by the E46K mutation, while the relative abundance of binding modes SL1 and SL2 is increased by the A30P and A53T mutations (Table 1). In the case of A30P αS, the SL1 binding mode even outnumbers the SL2 binding mode at low lipid concentrations, which represents an inversion from the wild-type populations. Although we are unable to directly measure the SL1 concentration in its relevant cellular environment, our data strongly suggest it to be impacted by the SL1:SL2 ratio. Figure 6 schematically illustrates how the SL1 binding mode, which anchors the N-terminus of αS in the lipoprotein complex while the more hydrophobic NAC region remains disordered, is prone to intermolecular interactions which may progress toward disease-associated oligomers and fibrils. We propose that the increase in SL1 levels, associated with the perturbation of the SL1:SL2 distribution, may contribute to the increased toxicity of the A30P and A53T disease variants of αS, whereas for the E46K variant, it is the higher membrane affinity that increases the SL1 concentration.

It has been previously documented that low lipid or detergent concentrations promote fibrilization of αS (*1*−*4*, *6*, *58*), citing as cause the increased local concentration of αS when many molecules compete for binding to a limited surface area. Indeed,

the duplication or triplication of the SNCA gene that encodes αS synuclein has also been correlated with genetic PD. The scheme proposed here extends this argument by highlighting the fact that lipid-limited conditions additionally promote a more aggregation-prone lipid binding mode of αS (SL1), while decreasing the level of conformations that may naturally work to offset aggregation propensity (SL2 or intermediate modes). Next to the increase in the relative concentration of fibril formation-prone SL1, it is important to note that the SL1 binding mode arranges the NAC region of these proteins (*59*, *60*) in a roughly parallel arrangement, promoting the formation of parallel β-sheet secondary structure observed for this region in amyloid fibrils (*61*). Therefore, when the molecules are lined up in-register, the risk for aggregation is particularly increased. The E46K variant, which overpopulates this binding mode, and the A30P and A53T variants, which elevate the SL1:SL2 ratio of binding modes relative to that of WT αS, all exhibit increased potential for this fibril-prone condition.

ACKNOWLEDGMENT

We thank James Masse, Nick Fitzkee, Frank Delaglio, and Alex Grishaev for help with data analysis and Danny Shang-Te Hsu for valuable help in the initial phase of this study.

SUPPORTING INFORMATION AVAILABLE

$^{1}H-^{15}N$ chemical shift assignments for disordered WT, A30P, E46K, and A53T αS; strip plots corresponding to the 3D HMQC-NOE-HMQC spectrum of A53T αS in the presence of dilute lipids; plot comparing WT αS HSQC attenuation in the presence of SUVs and LUVs; plots of HSQC attenuation for mixed samples of WT and A30P αS; and 1D ^{1}H spectra of phospholipids incorporated into SUVs versus LUVs. This material is available free of charge via the Internet at http://pubs.acs.org.

REFERENCES

1. Perrin, R. J., Woods, W. S., Clayton, D. F., and George, J. M. (2001) Exposure to long chain polyunsaturated fatty acids triggers rapid multimerization of synucleins. *J. Biol. Chem. 276*, 41958–41962.
2. Zhu, M., and Fink, A. L. (2003) Lipid binding inhibits α-synuclein fibril formation. *J. Biol. Chem. 278*, 16873–16877.
3. Zhu, M., Li, J., and Fink, A. L. (2003) The association of α-synuclein with membranes affects bilayer structure, stability, and fibril formation. *J. Biol. Chem. 278*, 40186–40197.
4. Necula, M., Chirita, C. N., and Kuret, J. (2003) Rapid anionic micelle-mediated α-synuclein fibrillization in vitro. *J. Biol. Chem. 278*, 46674–46680.
5. Welch, K., and Yuan, J. Y. (2003) α-Synuclein oligomerization: A role for lipids? *Trends Neurosci. 26*, 517–519.
6. Jo, E., Darabie, A. A., Han, K., Tandon, A., Fraser, P. E., and McLaurin, J. (2004) α-Synuclein-synaptosomal membrane interactions: Implications for fibrillogenesis. *Eur. J. Biochem. 271*, 3180–3189.
7. Lee, H. J., Choi, C., and Lee, S. J. (2002) Membrane-bound α-synuclein has a high aggregation propensity and the ability to seed the aggregation of the cytosolic form. *J. Biol. Chem. 277*, 671–678.
8. Cole, N. B., Murphy, D. D., Grider, T., Rueter, S., Brasaemle, D., and Nussbaum, R. L. (2002) Lipid droplet binding and oligomerization properties of the Parkinson's disease protein α-synuclein. *J. Biol. Chem. 277*, 6344–6352.
9. Lucke, C., Gantz, D. L., Klimtchuk, E., and Hamilton, J. A. (2006) Interactions between fatty acids and α-synuclein. *J. Lipid Res. 47*, 1714–1724.
10. Sharon, R., Bar-Joseph, I., Frosch, M. P., Walsh, D. M., Hamilton, J. A., and Selkoe, D. J. (2003) The formation of highly soluble oligomers of α-synuclein is regulated by fatty acids and enhanced in Parkinson's disease. *Neuron 37*, 583–595.
11. Polymeropoulos, M. H., Lavedan, C., Leroy, E., Ide, S. E., Dehejia, A., Dutra, A., Pike, B., Root, H., Rubenstein, J., Boyer, R., Stenroos, E. S., Chandrasekharappa, S., Athanassiadou, A., Papapetropoulos, T., Johnson, W. G., Lazzarini, A. M., Duvoisin, R. C., DiIorio, G., Golbe, L. I., and Nussbaum, R. L. (1997) Mutation in the α-synuclein gene identified in families with Parkinson's disease. *Science 276*, 2045–2047.
12. Kruger, R., Kuhn, W., Muller, T., Woitalla, D., Graeber, M., Kosel, S., Przuntek, H., Epplen, J. T., Schols, L., and Riess, O. (1998) Ala30Pro mutation in the gene encoding α-synuclein in Parkinson's disease. *Nat. Genet. 18*, 106–108.
13. Zarranz, J. J., Alegre, J., Gomez-Esteban, J. C., Lezcano, E., Ros, R., Ampuero, I., Vidal, L., Hoenicka, J., Rodriguez, O., Atares, B., Llorens, V., Tortosa, E. G., del Ser, T., Munoz, D. G., and de Yebenes, J. G. (2004) The new mutation, E46K, of α-synuclein causes Parkinson and Lewy body dementia. *Ann. Neurol. 55*, 164–173.
14. Spillantini, M. G., Crowther, R. A., Jakes, R., Hasegawa, M., and Goedert, M. (1998) α-Synuclein in filamentous inclusions of Lewy bodies from Parkinson's disease and dementia with Lewy bodies. *Proc. Natl. Acad. Sci. U.S.A. 95*, 6469–6473.
15. Spillantini, M. G., Schmidt, M. L., Lee, V. M. Y., Trojanowski, J. Q., Jakes, R., and Goedert, M. (1997) α-Synuclein in Lewy bodies. *Nature 388*, 839–840.
16. Conway, K. A., Harper, J. D., and Lansbury, P. T. (1998) Accelerated in vitro fibril formation by a mutant α-synuclein linked to early-onset Parkinson disease. *Nat. Med. 4*, 1318–1320.
17. El-Agnaf, O. M. A., Jakes, R., Curran, M. D., and Wallace, A. (1998) Effects of the mutations Ala(30) to Pro and Ala(53) to Thr on the physical and morphological properties of α-synuclein protein implicated in Parkinson's disease. *FEBS Lett. 440*, 67–70.
18. Narhi, L., Wood, S. J., Steavenson, S., Jiang, Y. J., Wu, G. M., Anafi, D., Kaufman, S. A., Martin, F., Sitney, K., Denis, P., Louis, J. C., Wypych, J., Biere, A. L., and Citron, M. (1999) Both familial Parkinson's disease mutations accelerate α-synuclein aggregation. *J. Biol. Chem. 274*, 9843–9846.
19. Li, J., Uversky, V. N., and Fink, A. L. (2001) Effect of familial Parkinson's disease point mutations A30P and A53T on the structural properties, aggregation, and fibrillation of human α-synuclein. *Biochemistry 40*, 11604–11613.
20. Choi, W., Zibaee, S., Jakes, R., Serpell, L. C., Davletov, B., Crowther, R. A., and Goedert, M. (2004) Mutation E46K increases phospholipid binding and assembly into filaments of human α-synuclein. *FEBS Lett. 576*, 363–368.
21. Greenbaum, E. A., Graves, C. L., Mishizen-Eberz, A. J., Lupoli, M. A., Lynch, D. R., Englander, S. W., Axelsen, P. H., and Giasson, B. I. (2005) The E46K mutation in α-synuclein increases amyloid fibril formation. *J. Biol. Chem. 280*, 7800–7807.
22. Pandey, N., Schmidt, R. E., and Galvin, J. E. (2006) The α-synuclein mutation E46K promotes aggregation in cultured cells. *Exp. Neurol. 197*, 515–520.
23. Volles, M. J., Lee, S. J., Rochet, J. C., Shtilerman, M. D., Ding, T. T., Kessler, J. C., and Lansbury, P. T. (2001) Vesicle permeabilization by protofibrillar α-synuclein: Implications for the pathogenesis and treatment of Parkinson's disease. *Biochemistry 40*, 7812–7819.
24. Volles, M. J., and Lansbury, P. T. (2002) Vesicle permeabilization by protofibrillar α-synuclein is sensitive to Parkinson's disease-linked mutations and occurs by a pore-like mechanism. *Biochemistry 41*, 4595–4602.
25. Lashuel, H. A., Petre, B. M., Wall, J., Simon, M., Nowak, R. J., Walz, T., and Lansbury, P. T. (2002) α-Synuclein, especially the Parkinson's disease-associated mutants, forms pore-like annular and tubular protofibrils. *J. Mol. Biol. 322*, 1089–1102.
26. Ding, T. T., Lee, S. J., Rochet, J. C., and Lansbury, P. T. (2002) Annular α-synuclein protofibrils are produced when spherical protofibrils are incubated in solution or bound to brain-derived membranes. *Biochemistry 41*, 10209–10217.
27. Adamczyk, A., and Strosznajder, J. B. (2006) α-Synuclein potentiates Ca^{2+} influx through voltage-dependent Ca^{2+} channels. *NeuroReport 17*, 1883–1886.
28. Zakharov, S. D., Hulleman, J. D., Dutseva, E. A., Antonenko, Y. N., Rochet, J. C., and Cramer, W. A. (2007) Helical α-synuclein forms highly conductive ion channels. *Biochemistry 46*, 14369–14379.
29. Kim, H. Y., Cho, M. K., Kumar, A., Maier, E., Siebenhaar, C., Becker, S., Fernandez, C. O., Lashuel, H. A., Benz, R., Lange, A., and Zweckstetter, M. (2009) Structural properties of pore-forming oligomers of α-synuclein. *J. Am. Chem. Soc. 131*, 17482–17489.
30. Conway, K. A., Lee, S. J., Rochet, J. C., Ding, T. T., Williamson, R. E., and Lansbury, P. T. (2000) Acceleration of oligomerization, not fibrillization, is a shared property of both α-synuclein mutations linked to early-onset Parkinson's disease: Implications for pathogenesis and therapy. *Proc. Natl. Acad. Sci. U.S.A. 97*, 571–576.

31. Lansbury, P. T. (1999) Evolution of amyloid: What normal protein folding may tell us about fibrillogenesis and disease. *Proc. Natl. Acad. Sci. U.S.A. 96*, 3342–3344.
32. Fredenburg, R. A., Rospigliosi, C., Meray, R. K., Kessler, J. C., Lashuel, H. A., Eliezer, D., and Lansbury, P. T. (2007) The impact of the E46K mutation on the properties of α-synuclein in its monomeric and oligomeric states. *Biochemistry 46*, 7107–7118.
33. Bussell, R., and Eliezer, D. (2001) Residual structure and dynamics in Parkinson's disease-associated mutants of α-synuclein. *J. Biol. Chem. 276*, 45996–46003.
34. Rospigliosi, C. C., McClendon, S., Schmid, A. W., Ramlall, T. F., Barre, P., Lashuel, H. A., and Eliezer, D. (2009) E46K Parkinson's-Linked Mutation Enhances C-Terminal-to-N-Terminal Contacts in α-Synuclein. *J. Mol. Biol. 388*, 1022–1032.
35. Bussell, R., and Eliezer, D. (2004) Effects of Parkinson's disease-linked mutations on the structure of lipid-associated α-synuclein. *Biochemistry 43*, 4810–4818.
36. Jensen, P. H., Nielsen, M. S., Jakes, R., Dotti, G., and Goedert, M. (1998) Binding of α-synuclein to brain vesicles is abolished by familial Parkinson's disease mutation. *J. Biol. Chem. 273*, 26292–26294.
37. Ulmer, T. S., and Bax, A. (2005) Comparison of structure and dynamics of micelle-bound human α-synuclein and Parkinson disease variants. *J. Biol. Chem. 280*, 43179–43187.
38. Stockl, M., Fischer, P., Wanker, E., and Herrmann, A. (2008) α-Synuclein selectively binds to anionic phospholipids embedded in liquid-disordered domains. *J. Mol. Biol. 375*, 1394–1404.
39. Bodner, C. R., Dobson, C. M., and Bax, A. (2009) Multiple tight phospholipid-binding modes of α-synuclein revealed by solution NMR spectroscopy. *J. Mol. Biol. 390*, 775–790.
40. Delaglio, F., Grzesiek, S., Vuister, G. W., Zhu, G., Pfeifer, J., and Bax, A. (1995) NMRpipe: A multidimensional spectral processing system based on Unix pipes. *J. Biomol. NMR 6*, 277–293.
41. Bermel, W., Bertini, I., Felli, I. C., Lee, Y. M., Luchinat, C., and Pierattelli, R. (2006) Protonless NMR experiments for sequence-specific assignment of backbone nuclei in unfolded proteins. *J. Am. Chem. Soc. 128*, 3918–3919.
42. Wang, C. Y., Rance, M., and Palmer, A. G. (2003) Mapping chemical exchange in proteins with MW > 50 kD. *J. Am. Chem. Soc. 125*, 8968–8969.
43. Igumenova, T. I., and Palmer, A. G. (2006) Off-resonance TROSY-selected R-1p experiment with improved sensitivity for medium- and high-molecular-weight proteins. *J. Am. Chem. Soc. 128*, 8110–8111.
44. Geen, H., and Freeman, R. (1991) Band-selective radiofrequency pulses. *J. Magn. Reson. 93*, 93–141.
45. Takamori, S., Holt, M., Stenius, K., Lemke, E. A., Gronborg, M., Riedel, D., Urlaub, H., Schenck, S., Brugger, B., Ringler, P., Muller, S. A., Rammner, B., Grater, F., Hub, J. S., De Groot, B. L., Mieskes, G., Moriyama, Y., Klingauf, J., Grubmuller, H., Heuser, J., Wieland, F., and Jahn, R. (2006) Molecular anatomy of a trafficking organelle. *Cell 127*, 831–846.
46. Bai, Y., Milne, J. S., and Englander, S. W. (1993) Primary structure effects on peptide group exchange. *Proteins 17*, 75–86.
47. Bertoncini, C. W., Jung, Y. S., Fernandez, C. O., Hoyer, W., Griesinger, C., Jovin, T. M., and Zweckstetter, M. (2005) Release of long-range tertiary interactions potentiates aggregation of natively unstructured α-synuclein. *Proc. Natl. Acad. Sci. U.S.A. 102*, 1430–1435.
48. Bernado, P., Bertoncini, C. W., Griesinger, C., Zweckstetter, M., and Blackledge, M. (2005) Defining long-range order and local disorder in native α-synuclein using residual dipolar couplings. *J. Am. Chem. Soc. 127*, 17968–17969.
49. Sung, Y. H., and Eliezer, D. (2007) Residual structure, backbone dynamics, and interactions within the synuclein family. *J. Mol. Biol. 372*, 689–707.
50. Ferreon, A. C. M., Gambin, Y., Lemke, E. A., and Deniz, A. A. (2009) Interplay of α-synuclein binding and conformational switching probed by single-molecule fluorescence. *Proc. Natl. Acad. Sci. U.S.A. 106*, 5645–5650.
51. Rhoades, E., Ramlall, T. F., Webb, W. W., and Eliezer, D. (2006) Quantification of α-synuclein binding to lipid vesicles using fluorescence correlation spectroscopy. *Biophys. J. 90*, 4692–4700.
52. Lee, J. C., Langen, R., Hummel, P. A., Gray, H. B., and Winkler, J. R. (2004) α-Synuclein structures from fluorescence energy-transfer kinetics: Implications for the role of the protein in Parkinson's disease. *Proc. Natl. Acad. Sci. U.S.A. 101*, 16466–16471.
53. Georgieva, E. R., Ramlall, T. F., Borbat, P. P., Freed, J. H., and Eliezer, D. (2008) Membrane-bound α-synuclein forms an extended helix: Long-distance pulsed ESR measurements using vesicles, bicelles, and rodlike micelles. *J. Am. Chem. Soc. 130*, 12856–12857.
54. Jao, C. C., Hegde, B. G., Chen, J., Haworth, I. S., and Langen, R. (2008) Structure of membrane-bound α-synuclein from site-directed spin labeling and computational refinement. *Proc. Natl. Acad. Sci. U.S.A. 105*, 19666–19671.
55. Drescher, M., Veldhuis, G., van Rooijen, B. D., Milikisyants, S., Subramaniam, V., and Huber, M. (2008) Antiparallel arrangement of the helices of vesicle-bound α-synuclein. *J. Am. Chem. Soc. 130*, 7796–7797.
56. Bortolus, M., Tombolato, F., Tessari, I., Bisaglia, M., Mammi, S., Bubacco, L., Ferrarini, A., and Maniero, A. L. (2008) Broken helix in vesicle and micelle-bound α-synuclein: Insights from site-directed spin labeling-EPR experiments and MD simulations. *J. Am. Chem. Soc. 130*, 6690–6691.
57. Eliezer, D., Kutluay, E., Bussell, R., and Browne, G. (2001) Conformational properties of α-synuclein in its free and lipid-associated states. *J. Mol. Biol. 307*, 1061–1073.
58. Rivers, R. C., Kumita, J. R., Tartaglia, G. G., Dedmon, M. M., Pawar, A., Vendruscolo, M., Dobson, C. M., and Christodoulou, J. (2008) Molecular determinants of the aggregation behavior of α- and *β*-synuclein. *Protein Sci. 17*, 887–898.
59. Bodles, A. M., Guthrie, D. J. S., Greer, B., and Irvine, G. B. (2001) Identification of the region of non-A*β* component (NAC) of Alzheimer's disease amyloid responsible for its aggregation and toxicity. *J. Neurochem. 78*, 384–395.
60. Giasson, B. I., Murray, I. V. J., Trojanowski, J. Q., and Lee, V. M. Y. (2001) A hydrophobic stretch of 12 amino acid residues in the middle of α-synuclein is essential for filament assembly. *J. Biol. Chem. 276*, 2380–2386.
61. Vilar, M., Chou, H. T., Luhrs, T., Maji, S. K., Riek-Loher, D., Verel, R., Manning, G., Stahlberg, H., and Riek, R. (2008) The fold of α-synuclein fibrils. *Proc. Natl. Acad. Sci. U.S.A. 105*, 8637–8642.